Reversible vector ratchets for skyrmion systems

X. Ma, C. J. Olson Reichhardt, and C. Reichhardt

Reversible Vector Ratchets for Skyrmion Assemblies

X. Ma[1,2], C. J. Olson Reichhardt[1], and C. Reichhardt[1]

[1] *Theoretical Division, Los Alamos National Laboratory,*
Los Alamos, New Mexico 87545 USA
[2] *Department of Physics, University of Notre Dame,*
Notre Dame, Indiana 46556 USA

We show that ac driven skyrmions interacting with an asymmetric substrate provide a realization of a new class of ratchet system which we call a vector ratchet that arises due to the effect of the Magnus term on the skyrmion dynamics. In a vector ratchet, the dc motion induced by the ac drive can be described as a vector that can be rotated clockwise or counterclockwise relative to the substrate asymmetry direction. Up to a full 360° rotation is possible for varied ac amplitudes or skyrmion densities. In contrast to overdamped systems, in which ratchet motion is always parallel to the substrate asymmetry direction, vector ratchets allow the ratchet motion to be in any direction relative to the substrate asymmetry. It is also possible to obtain a reversal in the direction of rotation of the vector ratchet, permitting the creation of a reversible vector ratchet. We examine vector ratchets for ac drives applied parallel or perpendicular to the substrate asymmetry direction, and show that reverse ratchet motion can be produced by collective effects. No reversals occur for an isolated skyrmion on an asymmetric substrate. Since a vector ratchet can produce motion in any direction, it could represent a new method for controlling skyrmion motion for spintronic applications.

I. INTRODUCTION

In a rocking ratchet, a particle or collection of particles interacting with an asymmetric substrate undergoes a net dc drift when subjected to an ac drive[1,2], as observed for vortices in type-II superconductors interacting with one-dimensional (1D)[3–5] or two-dimensional (2D) asymmetric substrates[6–9]. In the single particle limit, the ratchet motion is typically in the easy flow direction of the substrate asymmetry; however, when collective effects come into play, it is possible for a reverse ratchet effect to occur in which the particles move along the opposite or hard flow direction of the substrate asymmetry. Reversals of the ratchet direction can occur when parameters such as the ac amplitude, particle density, or substrate strength are varied[1,2,10–15]. It is also possible to observe a transverse ratchet effect in which the net dc drift of the particles is perpendicular to applied ac drive. For such transverse ratchets, when the ac drive is applied transverse to the substrate asymmetry direction, the resulting dc drift is parallel to the substrate asymmetry in either the easy or hard flow direction[11,16–18].

In many of the experimentally studied systems where ratchet effects occur, such as vortices in type-II superconductors[10,12,14,15,19] or colloids[20,21], the motion of the particles is effectively overdamped. Recently a new particlelike excitation called skyrmions was discovered in chiral magnets[22–24]. These skyrmions have many similarities to vortices in type-II superconductors in that they exhibit particlelike properties and have a mutually repulsive interaction that leads to the formation of a triangular skyrmion lattice[22,23]. Skyrmions can be driven with an applied current[24–30] and exhibit pinning-depinning phenomena[26,28,30]. A key difference between superconducting vortex and skyrmion systems is that in addition to the damping, skyrmion motion involves a strong non-dissipative Magnus effect which rotates the skyrmion velocity into the direction perpendicular to the net applied external forces. This Magnus term can be ten or more times larger than the damping term[24,26,28,31]. In the absence of pinning, under a dc drive the Magnus effect causes the skyrmions to move at an angle, the skyrmion Hall angle θ_{Sk}, with respect to the driving direction, where $\theta_{Sk} \sim \tan^{-1}(\alpha_m/\alpha_d)$ and α_m/α_d is the ratio of the Magnus term to the damping term. In the presence of pinning, the skyrmion Hall angle has a strong drive dependence[32–36]. Skyrmions have now been stabilized at room temperature[30,37,38] making them promising candidates for a variety of spintronic applications[39], any of which would require the ability to precisely control the skyrmion motion. One method for achieving such control would be to exploit ratchet effects.

In previous numerical work, it was shown that an individual skyrmion in a 2D system interacting with a quasi-1D asymmetric substrate exhibits a rocking ratchet effect when the ac drive is applied along the substrate asymmetry direction[40]. In this case, the resulting dc skyrmion velocity has components both parallel and perpendicular to the substrate asymmetry direction due to the Magnus term. A new type of ratchet effect, called a Magnus ratchet, was shown to occur when the ac drive is applied perpendicular to the substrate asymmetry direction[40]. Here, the Magnus term induces skyrmion velocity components both parallel and perpendicular to the ac drive. As a result, the skyrmions translate partially along the substrate asymmetry direction, permitting ratcheting motion to occur. In the overdamped limit, this Magnus ratchet effect is lost. In the single skyrmion limit for both longitudinal and transverse ac driving, the ratchet

flux is always aligned with the easy flow direction of the substrate asymmetry, so an open question is whether it is possible to realize a reversible skyrmion ratchet effect.

In this work we consider assemblies of skyrmions driven by ac forces over gradient pinning arrays. Previous studies of such arrays in the overdamped limit for superconducting vortices demonstrated that both longitudinal and transverse ratchet effects as well as ratchet reversals occur as a function of ac amplitude and vortex density[18,41]. Here we show that for ac drives applied either parallel or perpendicular to the substrate asymmetry direction, when a finite Magnus term is present, ratchet effects occur even in regimes where there is no ratchet motion in the overdamped limit, while multiple reversals of the ratchet effect can appear when the ac amplitude, the skyrmion density, or the ratio α_m/α_d of the Magnus term to the damping term is varied. The net dc drift of the skyrmions can be described as a vector which contains information about the magnitude of the drift and the angle between the drift direction and the substrate easy flow direction. With changing α_m/α_d, ac amplitude, or skyrmion density, the ratchet vector undergoes either a clockwise or counterclockwise rotation of up to 360°, indicating that ratcheting motion can occur in any direction for a 2D system. It is even possible to have a reversal in the direction of rotation of the ratchet vector. This system thus represents a new class of ratchet which we call a vector ratchet, and we predict that vector ratchets should be a general feature of any system in which Magnus effects are important, including skyrmions in chiral magnets[24], skyrmion phases in p-wave superconductors[42–44], rotating colloids[45], and charged particles in magnetic fields such as dusty plasmas[46,47]. Additionally, since vector ratchets allow for motion in any direction, they could serve as a new method to control skyrmion motion for spintronic applications. The skyrmion vector ratchet we describe here is distinct from ratchet effects observed in the single skyrmion limit[40], where no ratchet reversals appeared. The vector ratchet is a *collective* effect, with no ratcheting occurring in the single skyrmion limit, and with multiple ratchet reversals. Overall, the skyrmion vector ratchet exhibits a much richer variety of ratchet behavior than previously studied overdamped ratchets such as superconducting vortex ratchets.

II. SIMULATION

We model a 2D system of size $L \times L$ with periodic boundary conditions in the x- and y-directions containing N_s skyrmions at a density of $\rho_s = N_s/L^2$. We place N_p pinning sites in one of the periodic gradient array configurations illustrated in Fig. 1. We focus primarily on the conformal array shown in Fig. 1(a), which is produced by performing a conformal transformation on a uniform triangular array of pinning sites, as described in detail in previous work on pinning[48,49] and ratchet effects[18,41]
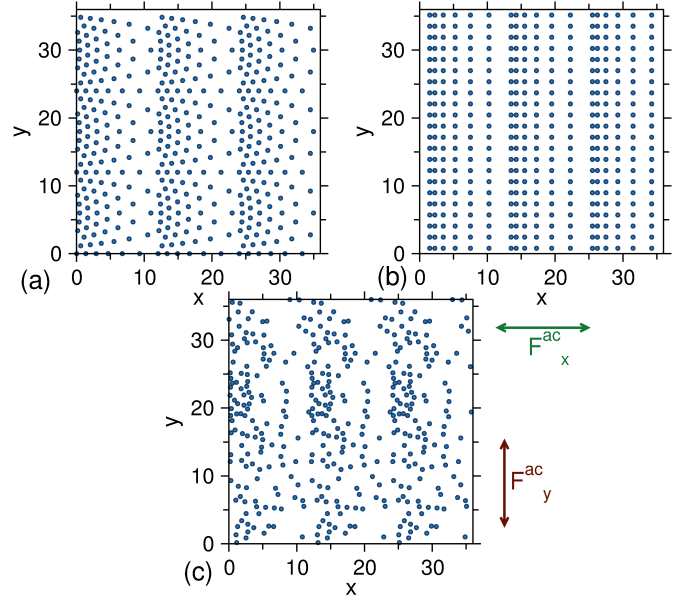

FIG. 1: Circles: Pinning site locations. (a) Conformal gradient array. (b) Square gradient array. (c) Random gradient array. Green arrow: direction of longitudinal drive F_x^{ac}. Red arrow: direction of transverse drive F_y^{ac}.

for superconducting vortices in conformal pinning arrays. Successful experimental realizations of conformal pinning arrays for superconducting vortex systems[50,51] suggest that similar nanofabrication techniques could be used to create such arrays for skyrmion systems. Figure 1(b) illustrates the square gradient array, produced by subjecting a square pinning lattice to a gradient along the x direction, while Fig. 1(c) shows the random gradient array, generated by introducing the same x direction pinning density gradient to a random pinning array. We apply an ac driving force to the skyrmions of either F_x^{ac}, in the longitudinal or x direction, or F_y^{ac}, in the transverse or y direction, and measure the average net displacement of the skyrmions as a function of ac cycle.

To simulate the skyrmion motion we use a modified Thiele equation[52] described in Refs.[31,33,34] that takes into account skyrmion-skyrmion interactions and skyrmion-pinning interactions. The equation of motion of a given skyrmion i is

$$\alpha_d \mathbf{v}_i + \alpha_m \hat{z} \times \mathbf{v}_i = \mathbf{F}_i^{ss} + \mathbf{F}_i^{sp} + \mathbf{F}^{ac}. \quad (1)$$

Here $\mathbf{r}_i$ is the location of skyrmion i and $\mathbf{v}_i = d\mathbf{r}_i/dt$ is the skyrmion velocity. The damping term with prefactor α_d generates a skyrmion velocity component in the direction of the net external forces, while the Magnus term with prefactor α_m generates a skyrmion velocity component perpendicular to the net external force direction. The repulsive skyrmion-skyrmion interactions are given by $\mathbf{F}_i^{ss} = \sum_{j=1}^{N_s} K_1(R_{ij})\hat{\mathbf{r}}$, where $R_{ij} = |\mathbf{r}_i - \mathbf{r}_j|$ is the distance between skyrmions i and j, and K_1 is the modified Bessel function which falls off exponentially for

large R_{ij}. The pinning force $\mathbf{F}_i^{sp}$ is modeled as arising from attractive nonoverlapping harmonic traps of radius R_p which can exert a maximum pinning force of F_p. The ac driving force is $\mathbf{F}^{ac} = F_\beta^{ac}\sin(\omega t)\hat{\beta}$, where $\beta = x$ for longitudinal driving and $\beta = y$ for transverse driving, as shown schematically in Fig. 1. To characterize the ratchet effect, we measure the average net displacement of the skyrmions over time in both the x and y directions to obtain $\langle \Delta X \rangle = N_s^{-1} \sum_{i=1}^{N_s}(x_i(t) - x_i(t_0))$ and $\langle \Delta Y \rangle = N_s^{-1} \sum_{i=1}^{N_s}(y_i(t) - y_i(t_0))$, where $(x_i, y_i)(t)$ is the position of skyrmion i at time t and t_0 is the initial reference time. We use a measurement interval of $t - t_0 = 400$ ac drive cycles, and the initial reference time t_0 is taken to be no less than 50 ac drive cycles after the system is initialized. The system size $L = 36$ and the spacing between repeated tilings of our gradient pinning arrays is $a_p = 12$. The average spacing between individual pinning sites is $a = 1.82$. In this work we focus on samples with skyrmion density $n_s = 0.3$, filling fraction of $n_s/n_p = 1.0$, pinning radius of $R_p = 0.3$, and pinning force of $F_p = 0.1$.

For comparison to experiments, the ratchet effect is most prominent for ac currents with a maximum amplitude that is larger than that of the dc critical depinning current. If we consider MnSi nanowires[29], which have depinning currents of approximately 10^8 A/m^2, the ratchet effects we observe should occur at ac current amplitudes in the range 0.5×10^8 to 8×10^8 A/m^2. The dc skyrmion velocities in these nanowires are on the order of 0.1 m^2/s. Since ratchet effects are generally most pronounced when a skyrmion can move a distance of at least one substrate lattice period a_p during a single ac cycle, the ac frequency ω should be smaller than the average skyrmion velocity divided by a_p. Thus in a sample with a ratchet substrate of periodicity $a_p = 500$ nm, ratchet effects should be observable for ac frequencies of 10^4 Hz or less.

We do not consider thermal fluctuations of the skyrmions, which could be a subject for future work. Previous studies of ratchet effects show that large thermal fluctuations generally destroy the ratchet effect, particularly when the ac drive amplitude is larger than the critical dc depinning current[6,7,41]. For ac amplitudes that are significantly smaller than the dc depinning threshold, thermal effects can instead increase the magnitude of the ratchet effect by permitting thermal excitation over the substrate barrier, and leading to the emergence of an optimum thermal noise level at which the magnitude of the ratchet effect is maximized[6,7]. We expect that similar thermal effects would arise for skyrmion ratchets. We also note that our approximation that the skyrmions can be treated as point particles breaks down when internal vibrational modes of the skyrmions become excited, which can occur at high drives or when the skyrmions are very large.
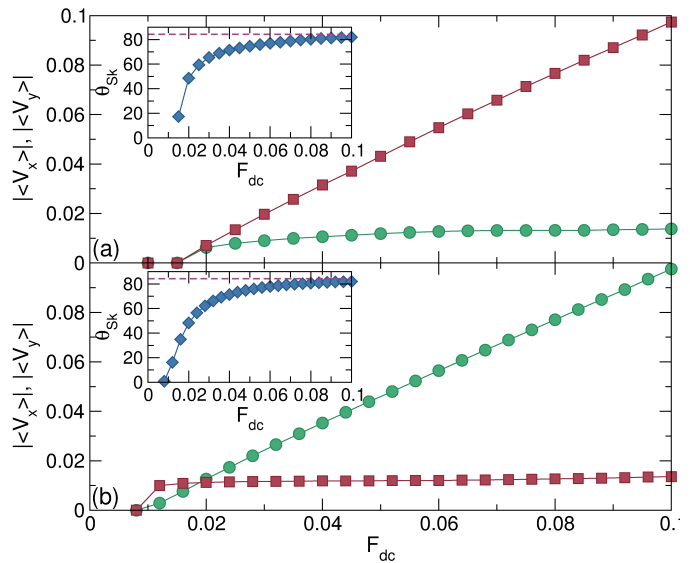

FIG. 2: The velocity-force curves $|\langle V_x \rangle|$ (green circles) and $|\langle V_y \rangle|$ (red squares) vs dc drive F_{dc} for the conformal pinning array in Fig. 1(a) with a skyrmion density of $n_s = 0.3$ and $\alpha_m/\alpha_d = 9.962$. (a) For dc driving in the positive x direction, the critical depinning threshold is $F_c \approx 0.015$. Inset: The skyrmion Hall angle $\theta_{Sk} = \tan^{-1}(|\langle V_\perp \rangle|/|\langle V_{||} \rangle|)$ vs dc drive amplitude F_{dc}, where $V_\perp = V_y$ and $V_{||} = V_x$. The dashed line indicates the pin free limit of $\theta_{Sk} = 84.267°$. (b) For dc driving in the positive y direction, close to the depinning threshold the skyrmion motion is strongly guided along the y direction by the pinning sites. Inset: θ_{Sk} vs F_{dc}, where $V_\perp = V_x$ and $V_{||} = V_y$, shows that θ_{Sk} is nearly zero at low drives and increases with increasing F_{dc}. The dashed line indicates the pin free limit of $\theta_{Sk} = 84.267°$.

III. DC DEPINNING

We first apply a dc drive to the conformal pinning array sample in order to determine the depinning threshold. In Fig. 2(a) we plot $|\langle V_x \rangle|$ and $|\langle V_y \rangle|$ versus the dc drive amplitude F_{dc} for driving in the positive x-direction in a sample with $\alpha_m/\alpha_d = 9.962$. The inset shows the skyrmion Hall angle $\theta_{Sk} = \tan^{-1}(|\langle V_\perp \rangle|/|\langle V_{||} \rangle|)$ versus F_{dc}, where $V_\perp = V_y$ and $V_{||} = V_x$. The depinning threshold F_c is close to $F_c = 0.015$. The Hall angle $\theta_{Sk} \approx 20°$ at low drives, and gradually increases with increasing F_{dc} until it reaches the expected pin-free value of $\theta_{Sk} = 84.267°$. This strong dependence of the skyrmion Hall angle on the external drive in the presence of pinning was observed in previous studies of particle-based[33,34] and continuum-based[32] simulations as well as in experiments[35]. For dc driving in the positive y direction, Fig. 2(b) shows that the depinning threshold has a lower value of $F_c = 0.01$. Near depinning, there is a stronger guiding effect in the y-direction as the skyrmions move through the low pinning density region of the conformal array. As a result, the motion just above depinning is almost completely locked in the y direction, giving a Hall angle close to zero, as shown in the inset of
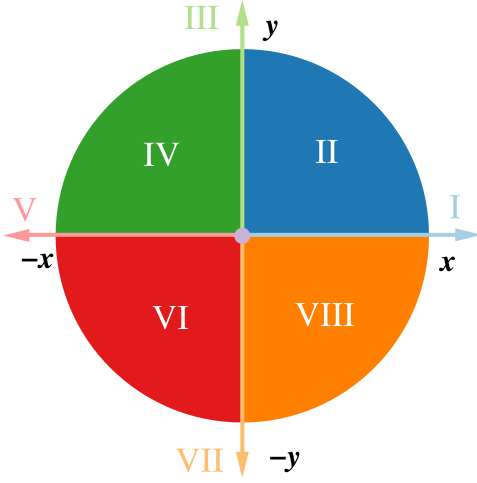
FIG. 3: A diagram showing the eight possible types of vector ratchet motion for the conformal pinning array in Fig. 1(a). The net dc drift in the (x, y) direction for each type is: I: $(+x, 0)$ (light blue); II: $(+x, +y)$ (dark blue); III: $(0, +y)$ (light green); IV: $(-x, +y)$ (dark green); V: $(-x, 0)$ (pink); VI: $(-x, -y)$ (red); VII $(0, -y)$ (light orange); and VIII $(+x, -y)$ (dark orange). In addition, we define type IX with $(0, 0)$ (purple) to be a state with no ratcheting motion.
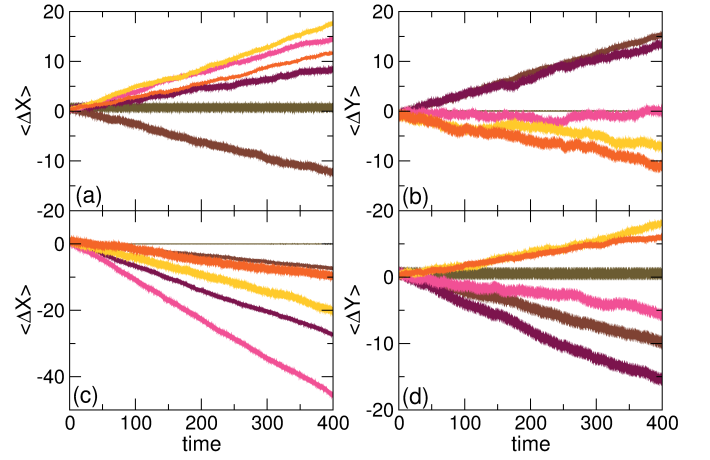
Fig. 2(b).

FIG. 4: (a,b) The average cumulative displacement per skyrmion $\langle \Delta X \rangle$ (a) and $\langle \Delta Y \rangle$ (b) vs time in ac cycles for the conformal pinning array under longitudinal ac driving with $n_s = 0.3$ and $F_x^{ac} = 0.04$ at $\alpha_m/\alpha_d = 0$ (dark green), 1.36 (dark brown), 4.0 (burgundy), 8.0 (dark pink), 10 (yellow), and 20 (orange). There is no ratchet motion when $\alpha_m/\alpha_d = 0$, but for $\alpha_m/\alpha_d \neq 0$, we observe ratchet reversals in both the x and y directions. (c,d) $\langle \Delta X \rangle$ (c) and $\langle \Delta Y \rangle$ (d) vs time in ac cycles for the same system for transverse ac driving at $F_y^{ac} = 0.04$ and $\alpha_m/\alpha_d = 0$ (dark green), 1.2 (dark brown), 1.6 (burgundy), 2.6 (dark pink), 10 (yellow), and 20 (orange). In this case the ratchet motion for $\alpha_m/\alpha_d \neq 0$ is always in the negative x direction and shows a reversal in the y direction.

IV. RATCHET EFFECTS WITH LONGITUDINAL AND TRANSVERSE AC DRIVES

To analyze the ratchet effect, we apply an ac drive to the conformal pinning array sample in Fig. 1(a) along the longitudinal (F_x^{ac}) or transverse (F_y^{ac}) direction, as indicated by the arrows in Fig. 1, for a skyrmion density of $n_s = 0.3$. In the overdamped case, only two types of ratchet effects occur: a net dc motion along the positive or negative x direction, parallel to the drive, for longitudinal driving, and a net dc motion along the positive or negative x direction, perpendicular to the drive, for transverse driving. In contrast, there can be up to eight types of motion for a Magnus induced ratchet. As shown in Fig. 3, these are type I, with net motion in the positive x direction only; type II, with net motion in the positive x and positive y directions; type III, with net motion in the positive y direction only; type IV, with net motion in the negative x and positive y directions; type V, with net motion in the negative x direction only; type VI, with net motion in the negative x and negative y directions; type VII, with net motion in the negative y direction only; and type VIII, with net motion in the positive x and negative y directions. We also refer to type IX, where there is no net motion in either direction, indicating the lack of a ratchet effect. Overdamped systems exhibit ratchet types I and V.

We now consider a case where there is no ratchet ef-

fect in the overdamped limit for either longitudinal or transverse ac driving, and we vary the ratio α_m/α_d of the Magnus term to the damping term. In Fig. 4(a,b) we plot the average cumulative displacement per skyrmion $\langle \Delta X \rangle$ in the x direction and $\langle \Delta Y \rangle$ in the y direction versus time in ac cycles for a system with $F_x^{ac} = 0.04$ in the longitudinal or x direction. At $\alpha_m/\alpha_d = 0$, $\langle \Delta X \rangle = 0$ and $\langle \Delta Y \rangle = 0$, indicating the absence of a ratchet effect. For $\alpha_m/\alpha_d = 1.36$, the skyrmions move in the negative x direction and the positive y direction, which in the notation of Fig. 3 is a type IV ratchet. The negative x direction is the easy flow direction of the substrate asymmetry. As α_m/α_d increases from 4 to 20, a reversal of the ratchet effect occurs in which $\langle \Delta X \rangle$ becomes positive so that the skyrmions are moving in the hard flow direction of the substrate asymmetry. The corresponding $\langle \Delta Y \rangle$ remains in the positive y direction for $\alpha_m/\alpha_d = 4$, resulting in a type II ratchet, while for $\alpha_m/\alpha_d = 8.0$, $\langle \Delta X \rangle > 0$ and $\langle \Delta Y \rangle = 0$, giving a type I ratchet. For $\alpha_m/\alpha_d = 10$ and 20, there is a y direction reversal with $\langle \Delta Y \rangle < 0$ and $\langle \Delta X \rangle > 0$, producing a type VIII ratchet. The sequence of ratchet types that appear as a function of increasing α_m/α_d, including the lack of a ratchet effect at $\alpha_m/\alpha_d = 0$, is IX-IV-III-II-I-VIII, so that the ratchet direction is moving clockwise around the diagram in Fig. 3.

In Fig. 4(c,d) we show $\langle \Delta X \rangle$ and $\langle \Delta Y \rangle$ versus time in ac cycles for transverse or y direction ac driving with
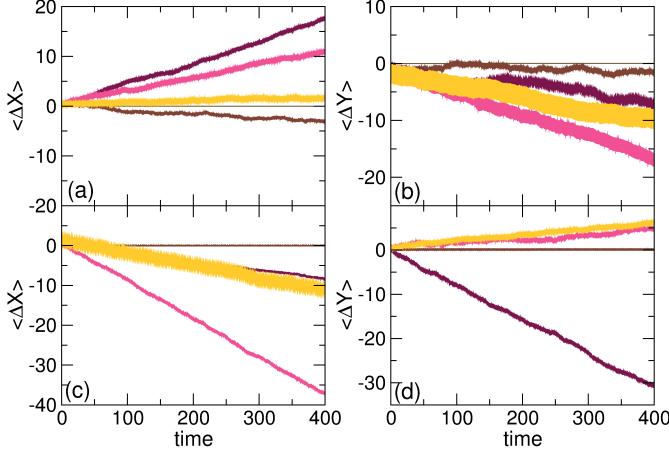
FIG. 5: (a,b) $\langle \Delta X \rangle$ (a) and $\langle \Delta Y \rangle$ (b) vs time in ac cycles for the conformal pinning array for longitudinal ac driving with $\alpha_m/\alpha_d = 10$ at $F_x^{ac} = 0$ (gray), 0.025 (brown), 0.04 (burgundy), 0.06 (pink), and 0.08 (orange). There is no ratchet motion at $F_x^{ac} = 0$, but for $F_x^{ac} > 0$, ratchet reversals occur in both the x and y directions. (c,d) $\langle \Delta X \rangle$ (c) and $\langle \Delta Y \rangle$ (d) for the same system for transverse ac driving at $\alpha_m/\alpha_d = 10$ and $F_y^{ac} = 0$ (gray), 0.007 (brown), 0.015 (burgundy), 0.021 (pink), and 0.06 (orange). The ratchet effect is always in the negative x direction and shows a reversal in the y direction.
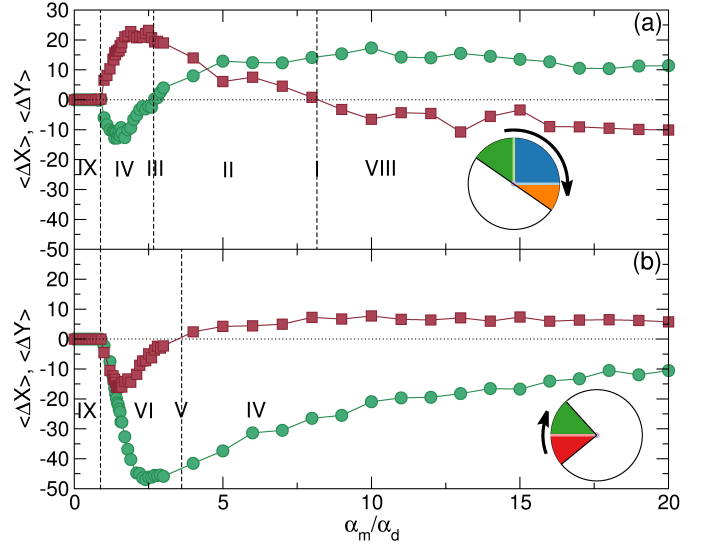

FIG. 6: The value of $\langle \Delta X \rangle$ (green circles) and $\langle \Delta Y \rangle$ (red squares) after 400 ac cycles vs α_m/α_d for the system in Fig. 4. (a) Driving in the x direction with $F_x^{ac} = 0.04$. The ratchet sequence is IX-IV-III-II-I-VIII, so that the flow rotates clockwise by 180° as indicated in the inset, which is based on the schematic in Fig. 3. (b) Driving in the y direction with $F_y^{ac} = 0.04$. The ratchet sequence is IX-VI-V-IV giving a counterclockwise rotation of 90° as shown in the inset.

$F_y^{ac} = 0.04$, where there is again no ratchet effect for $\alpha_m/\alpha_d = 0$. We find that $\langle \Delta X \rangle$ is always negative but that there is a reversal in $\langle \Delta Y \rangle$, which is negative for $0 < \alpha_m/\alpha_d < 10$, giving a type VI ratchet, and positive for $\alpha_m/\alpha_d \geq 10$, producing a type IV ratchet. The ratchet sequence in this case is IX-VI-V-IV. The maximum ratchet flow magnitude is 3.75 times larger for transverse ac driving than for longitudinal ac driving.

We also observe ratchet reversals at fixed $\alpha_m/\alpha_d = 9.962$ as we vary F_x^{ac}, as shown in Fig. 5(a,b) where we plot $\langle \Delta X \rangle$ and $\langle \Delta Y \rangle$ versus time in ac cycles. At $F_x^{ac} = 0$ there is no ratchet effect, while at $F_x^{ac} = 0.025$, there is a weak ratchet effect in the negative x direction that crosses over to a positive x ratchet for $F_x^{ac} = 0.04$ and 0.06. The ratchet effect in the y-direction is always negative. At $F_x^{ac} = 0.08$, the motion is predominately in the negative y direction with almost no x direction movement, so the resulting sequence of ratchet types is IX-V-VIII-VI.

In Fig. 5(c,d) we show $\langle \Delta X \rangle$ and $\langle \Delta Y \rangle$ versus time for the $\alpha_m/\alpha_d = 9.962$ sample under transverse ac driving. The ratchet effect is always in the negative x direction, with the largest ratchet flow occurring at $F_y^{ac} = 0.021$, a drive at which a given skyrmion translates a distance larger than the entire system length L during half of an ac drive cycle. The ratchet motion transitions from weak to strong negative y direction flow with increasing F_y^{ac} before switching to positive y direction flow for $F_y^{ac} > 0.02$, giving a ratchet sequence of IX-VI-V-IV.

In Fig. 6(a) we plot the values of $\langle \Delta X \rangle$ and $\langle \Delta Y \rangle$ after 400 ac cycles as a function of α_m/α_d for the system in Fig. 4(a,b). At $\alpha_m/\alpha_d = 0$ there is no ratchet ef-

fect, which we term a type IX ratchet, while for $0.75 < \alpha_m/\alpha_d < 2.6$, the ratchet motion is in the negative x and positive y directions, which is a type IV ratchet. The ratchet motion passes through zero in the x direction at $\alpha_m/\alpha_d = 2.6$ while continuing to flow in the positive y direction, giving a type III ratchet. This is also an example of a transverse ratchet effect in which a longitudinal dc drive produces drift motion strictly in the transverse direction. In the interval $2.6 < \alpha_m/\alpha_d < 8.0$ we find a type II ratchet with positive x and positive y motion, followed by a type I or strictly positive x direction ratchet at $\alpha_m/\alpha_d = 8.0$. Finally, for $\alpha_m/\alpha_d > 8.0$, we observe type VIII flow with positive x and negative y motion. The sequence of ratchet types as a function of α_m/α_d is indicated in the inset of Fig. 6(a), where the flow begins in region IV and gradually rotates clockwise by nearly 180°. For driving in the y direction, Fig. 6(b) shows that initially the system exhibits a type VI ratchet effect with negative x and y motion, passes through a type V ratchet in which motion occurs only in the negative x direction despite the fact that the driving is applied along the y direction, and then finally enters a broad type IV ratchet region in which the flow is in the negative x and positive y directions. The flow sequence is thus IX-VI-V-IV, and the flow rotates clockwise in the inset of Fig. 6(b) by about 90° as a function of α_m/α_d.

In Fig. 7(a) we plot $\langle \Delta X \rangle$ and $\langle \Delta Y \rangle$ versus F_x^{ac} for the system in Fig. 4 under x direction driving with $\alpha_m/\alpha_d = 10.0$. A series of ratchet types appear, and there is a double reversal in $\langle \Delta Y \rangle$ from negative to posi-
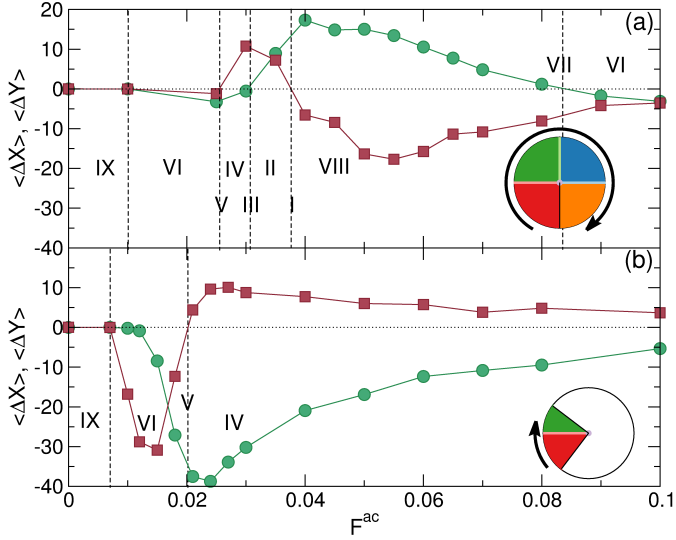
FIG. 7: $\langle \Delta X \rangle$ (green circles) and $\langle \Delta Y \rangle$ (red squares) after 400 ac cycles vs F^{ac} for the system in Fig. 4 at $\alpha_m/\alpha_d = 10.0$. (a) Driving in the x direction with F_x^{ac}. The ratchet sequence is IX-VI-V-IV-III-II-I-VIII-VII-VI, giving a clockwise rotation of $360°$ as indicated in the inset. (b) Driving in the y direction with F_y^{ac}. The ratchet sequence is IX-VI-V-IV, giving a clockwise rotation of $90°$, as shown in the inset.
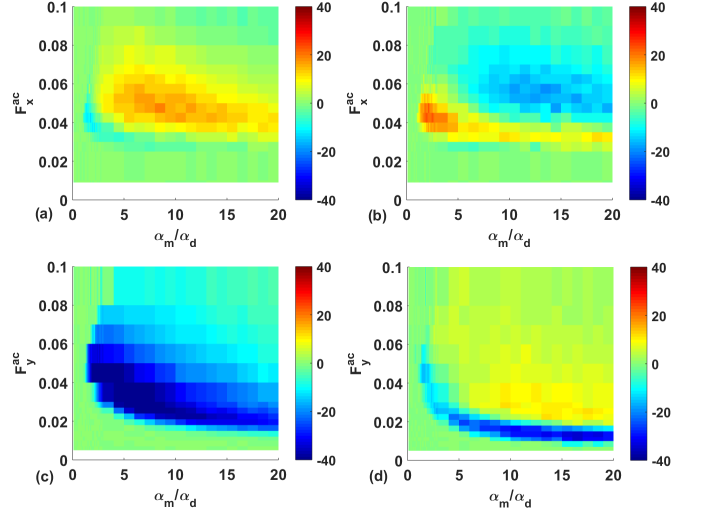

FIG. 8: Heat maps of (a) $\langle \Delta X \rangle$ and (b) $\langle \Delta Y \rangle$ as a function of F_x^{ac} vs α_m/α_d for the conformal array. Here there are ratchet reversals in both the x and y directions. (c) Heat map of $\langle \Delta X \rangle$ for driving in the y-direction where the drift is always in the negative x direction. (d) The corresponding $\langle \Delta Y \rangle$ as a function of F_y^{ac} vs α_m/α_d showing a reversal.

tive and then back to negative, as well as in $\langle \Delta X \rangle$, which transitions from negative to positive and back to negative. The resulting ratchet sequence is IX-VI-V-IV-III-II-I-VIII-VII-VI, showing that the flow undergoes clockwise rotation through all the possible ratchet types or a rotation of $360°$ in the inset of Fig. 7(a). For y direction driving, F_y^{ac}, Fig. 7(b) shows that the ratchet sequence is IX-VI-V-IV, giving a clockwise rotation of $90°$.

From the ratchet behavior shown in Figs. 6 and 7, we can describe the direction of ratchet motion in terms of a vector with an amplitude of $R = |\langle \Delta X \rangle^2 + \langle \Delta Y \rangle^2|^{1/2}$ and an orientation of θ. This ratchet vector rotates as the parameters of the system are changed, and it can in principle point along any direction θ in the $x-y$ plane even though the asymmetry of the substrate exists only along the x-direction. This represents a new type of ratchet that arises due to the skyrmion Hall angle, which depends on both α_m/α_d and drive amplitude as shown in Fig. 2. For the parameters we consider, increasing the ac drive or the ratio α_m/α_d increase the skyrmion Hall angle in the clockwise direction.

In order to get a better understanding of the evolution of the ratchet flow in Figs. 6 and 7, in Fig. 8 we show a heat map of the direction and magnitude of the net flux for x direction ac driving based on the value of $\langle \Delta X \rangle$ (Fig.8(a)) and $\langle \Delta Y \rangle$ (Fig.8(b)) after 400 ac cycles as a function of F_x^{ac} vs α_m/α_d. Here for $F_x^{ac} < 0.3$ and $F_x^{ac} > 0.9$, the ratchet effect is weak or absent. It is also clear that a reversal occurs in both $\langle \Delta X \rangle$ and $\langle \Delta Y \rangle$ as functions of α_m/α_d and F_x^{ac}. Figure 8(d,e) shows similar heat maps for y direction ac driving. In this case

the maximum intensity of the ratchet effect is stronger and $\langle \Delta X \rangle$ is always negative, while there is a reversal in $\langle \Delta Y \rangle$. Since $\langle \Delta X \rangle$ is always negative, the ratchet sequence is limited to types III-IV-V-VI-VII.

V. SKYRMION DENSITY DEPENDENCE AND COMMENSURATION EFFECTS

We next consider the effect of varying the skyrmion density for a fixed pinning site density of $n_p = 0.3$ at $\alpha_m/\alpha_d = 9.962$. In Fig. 9(a) we plot $\langle \Delta X \rangle$ and $\langle \Delta Y \rangle$ after 400 ac cycles for x direction driving of $F_x^{ac} = 0.05$ with $F_p = 0.1$ over the range $0 < n_s/n_p < 2.0$. There is a strong type VIII ratchet flux for $n_s/n_p > 0.7$, and the ratchet sequence IV-III-II-I-VIII progresses clockwise around the diagram in the inset of Fig. 9(a). In general we do not observe any ratchet motion in the single skyrmion limit of $n_s/n_p \approx 0$, indicating that the skyrmion ratchet motion on the conformal array is a *collective* effect, unlike the ratchet effect observed for a single skyrmion on a quasi-one-dimensional asymmetric substrate[40]. There is a weak dip in the ratchet flux at $n_s/n_p = 1.0$, and the maximum ratchet flux occurs near $n_s/n_p = 1.5$, above which the flux decreases again. In general, the ratchet flux diminishes for large n_s/n_p where the skyrmions form a stiff lattice that only weakly couples to the substrate. Similar effects appear in a superconducting vortex system for the ratchet flux at high vortex densities in the presence of a conformal pinning array[41]. In Fig. 9(b) we show the same system with y direction driving of $F_y^{ac} = 0.05$. For $n_s/n_p < 0.5$, the data is fairly
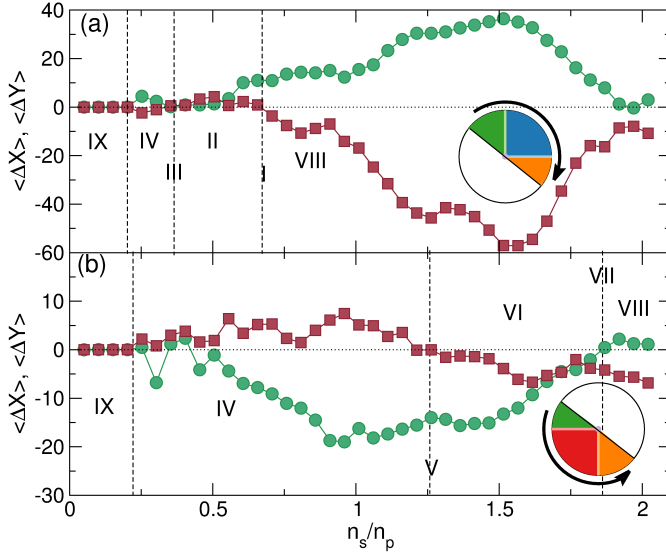
FIG. 9: $\langle \Delta X \rangle$ (green circles) and $\langle \Delta Y \rangle$ (red squares) after 400 ac cycles vs skyrmion density n_s/n_p for $F_p = 0.1$, $F^{ac} = 0.05$, and $\alpha_m/\alpha_d = 9.962$. (a) Driving in the x direction, F_x^{ac}. (b) Driving in the y direction, F_y^{ac}.
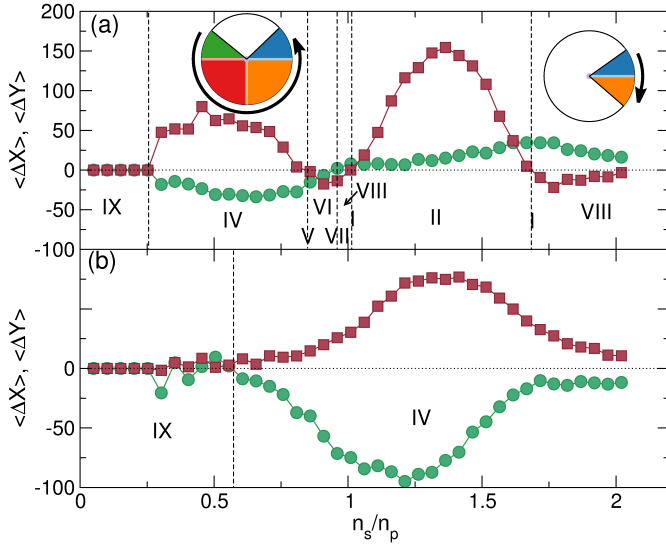

FIG. 10: $\langle \Delta X \rangle$ (green circles) and $\langle \Delta Y \rangle$ (red squares) after 400 ac cycles vs skyrmion density n_s/n_p for $F_p = 0.5$, $F^{ac} = 0.25$ and $\alpha_m/\alpha_d = 9.962$. (a) Driving in the x direction, F_x^{ac}. The ratchet flow direction initially rotates counterclockwise, followed by a clockwise rotation for $n_s/n_p > 1.3$. (c) Driving in the y direction, F_y^{ac}.

noisy, but for $n_s/n_p > 0.5$, ratchet flow occurs in both $\langle \Delta X \rangle$ and $\langle \Delta Y \rangle$ with a ratchet sequence of IX-IV-V-VI-VII-VIII, indicating a counter-clockwise rotation of the flow by 180° as indicated in the inset.

In Fig. 10(a) we show the same system as in Fig. 9(a) driven in the x-direction with a pinning strength of $F_p = 0.5$ and an ac amplitude of $F_x^{ac} = 0.25$ that have both
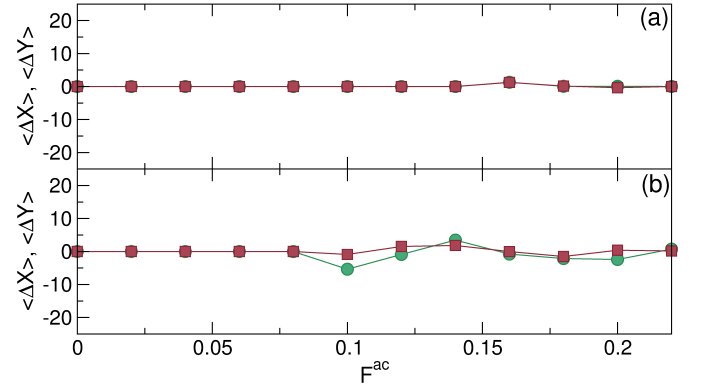

FIG. 11: $\langle \Delta X \rangle$ (green circles) and $\langle \Delta Y \rangle$ (red squares) for a single skyrmion, $N_s = 1$, after 400 ac cycles vs F^{ac} for $F_p = 0.1$ and $\alpha_m/\alpha_d = 9.962$. (a) Driving in the x direction, where there is no ratchet effect. (b) Driving in the y direction, where there is a very weak ratchet effect for $F^{ac}/F_p > 1.0$.

been increased by a factor of five. In this case, the net ratchet flux is up to 3.75 times larger than that produced when $F_x^{ac} = 0.05$ and $F_p = 0.1$. Here, $\langle \Delta Y \rangle$ is generally larger than $\langle \Delta X \rangle$, and there are multiple reversals in the y direction motion as well as one reversal in the x direction motion. The ratchet sequence is IX-IV-V-VI-VII-VIII-I-II for $n_s/n_p < 1.25$, giving a counter-clockwise rotation of the flow direction by 270° as shown in the leftmost inset of Fig. 9(a), while for $n_s/n_p > 1.25$, the ratchet sequence is II-I-VIII, giving a clockwise rotation of 90° as shown in the rightmost inset. This indicates that it is also possible to have reversals in the direction of the ratchet flow rotation, leading to what we term a reversible vector ratchet. Near $n_s/n_p = 1.0$, the ratchet flux is strongly reduced due to enhanced pinning from a commensuration effect with the underlying substrate. In Fig. 10(b), we show the ratchet flux in the same system for driving in the y-direction with $F_y^{ac} = 0.25$. There is a strong type IV ratchet effect with a maximum flux near $n_s/n_p = 1.25$. These results show that the skyrmion ratchet effect is robust over a wide range of skyrmion densities, ac drive amplitudes, and α_m/α_d ratios.

In Fig. 10, the ratchet effect vanishes as the skyrmion density decreases to zero, indicating the absence of a skyrmion ratchet effect in the single skyrmion limit. We have simulated the $N_s = 1$ single skyrmion limit for a wide range of parameters including varied α_m/α_d for ac driving in either the x or y-direction, and find that there is little to no ratchet effect in this regime. In Fig. 11(a) we plot $\langle \Delta X \rangle$ and $\langle \Delta Y \rangle$ after 400 ac cycles versus F_x^{ac} for the same system shown in Fig. 7 with $F_p = 0.1$ and only a single skyrmion present. There is no ratchet effect in the entire range $0 < F_x^{ac}/F_p < 2.0$. For y direction driving, Fig. 11(b) shows that only a very weak ratchet effect appears in the single skyrmion limit for $F_y^{ac}/F_p > 1.0$.

We have also examined the effect of varying the ac driving frequency. In Fig. 12(a,b) we plot $\langle \Delta X \rangle$ and $\langle \Delta Y \rangle$ after 400 ac cycles versus ac frequency ω in sam-
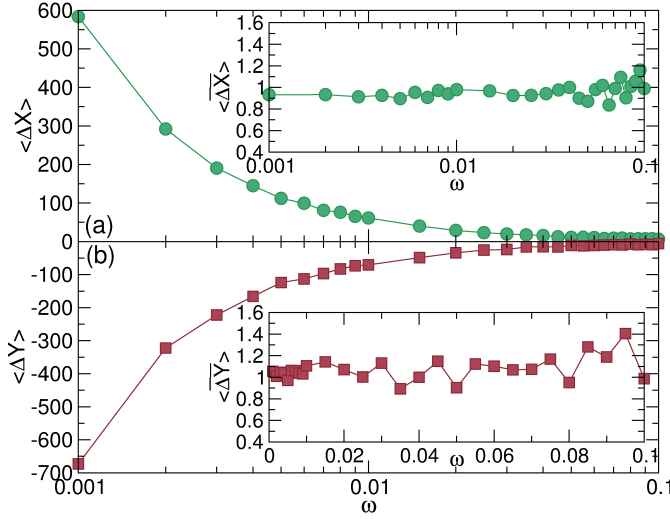
FIG. 12: (a) $\langle \Delta X \rangle$ (green circles) and (b) $\langle \Delta Y \rangle$ (red squares) after 400 ac cycles vs ac frequency ω in samples with $\alpha_m/\alpha_d = 9.962$ and $F_x^{ac} = 0.05$. In both cases, the ratchet flux decreases with increasing ac drive frequency. The insets show normalized values (a) $\langle \overline{\Delta X} \rangle$ and (b) $\langle \overline{\Delta Y} \rangle$ vs ω. Normalization is achieved by dividing by the total time required to perform 400 ac drive cycles at each frequency, and then dividing by the value at $\omega = 0.04$.

ples with $n_s/n_p = 0.3$ and $\alpha_m/\alpha_d = 9.962$. The ratchet flux drops with increasing ω, in agreement with observations made in overdamped systems[41]. In the insets of Fig. 12(a,b), we show the normalized quantities $\langle \overline{\Delta X} \rangle = \langle \Delta X \rangle/X_0\tau(\omega)$ and $\langle \overline{\Delta Y} \rangle = \langle \Delta Y \rangle/Y_0\tau(\omega)$, where $\tau(\omega)$ is the number of simulation time steps required to complete 400 ac drive cycles at a driving frequency ω, X_o is the value of $\langle \Delta X \rangle/\tau(\omega)$ at $\omega = 0.04$, and Y_o is the value of $\langle \Delta Y \rangle/\tau(\omega)$ at $\omega = 0.04$. The normalized measures indicate that the net ratchet flux remains roughly constant when adjusted for the amount of time spent ratcheting at the different ac drive frequencies.

VI. PARTICLE TRAJECTORIES

We image the skyrmion trajectories on either side of a ratchet reversal in order to understand how the geometry of the pinning array affects the skyrmion motion and how the amplitude of the ac drive can change the direction of the net ratchet flux. In Fig. 13(a,b) we plot the skyrmion positions, pinning site locations, and skyrmion trajectories in a sample with $\alpha_m/\alpha_d = 9.962$ and $n_s = n_p = 0.3$ under a y direction ac drive of $F_y^{ac} = 0.013$, which produces a type VI ratchet with strong flux in the negative y direction and weak flux in the negative x direction. During the positive portion of the ac drive cycle, shown in Fig. 13(a), the skyrmions predominantly move in the positive y direction. The flow is concentrated in the regions of lower pinning density, and there is a small amount of skyrmion hopping in the positive x direction, which is
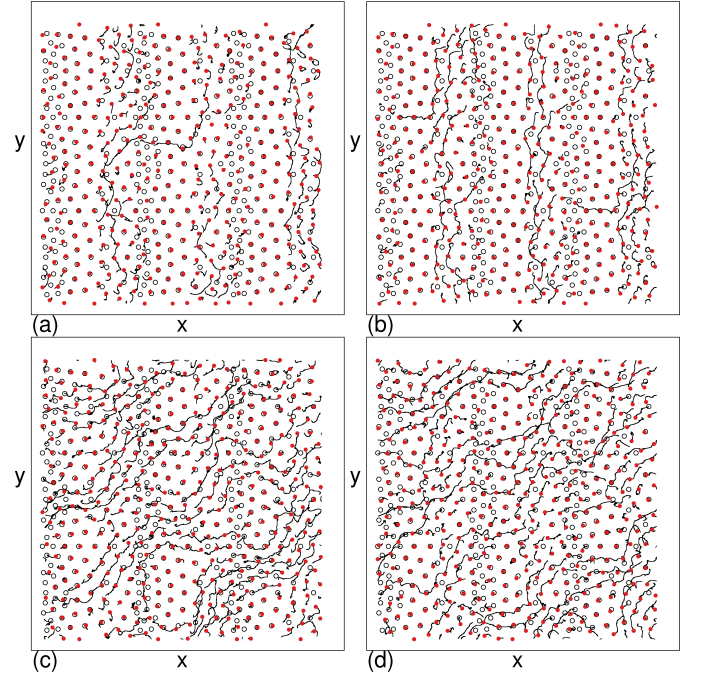

FIG. 13: Skyrmion positions (filled dots), pinning site locations (open circles), and trajectories (lines) for y direction ac driving F_y^{ac} in a sample with $n_s/n_p = 1.0$. (a) The positive ac drive cycle for $F_y^{ac} = 0.013$. (b) The negative ac drive cycle for $F_y^{ac} = 0.013$. At this drive, a type VI ratchet with motion in the negative y and negative x directions occurs. (a) The positive ac drive cycle for $F_y^{ac} = 0.03$. (a) The negative ac drive cycle for $F_y^{ac} = 0.03$. Here, there is a type IV ratchet with motion in the negative x and positive y directions.

the hard flow direction of the substrate asymmetry. If the pinning sites were not present, during the positive portion of the ac drive cycle the skyrmions would move with a Hall angle of 85° relative to the positive y axis. Instead, in Fig. 13(a), the Hall angle is nearly zero since skyrmion motion in the positive x direction is blocked by the regions of dense pinning. The Magnus term couples the x and y motion and causes the positive y direction to act like a hard flow direction even though there is no asymmetry in the substrate along the y direction. During the negative portion of the ac drive cycle, illustrated in Fig. 13(b), the motion is mostly in the negative y direction, with some hopping in the negative x direction. Since the negative x direction is the easy flow direction of the ratchet asymmetry, the Magnus coupling causes the negative y direction to act like an easy flow direction, and the net ratchet flux during the entire cycle is larger in the negative y direction than in the positive y direction, producing a net negative y and negative x flow. Figure 13(c) shows the positive portion of the ac cycle for a drive of $F_y^{ac} = 0.03$, while Fig. 13(d) shows the negative portion of the ac cycle at the same drive. For this ac drive amplitude, there is a strong ratchet flux in the negative x direction and a weaker ratchet flux in the positive y direction, giving a type IV ratchet effect.
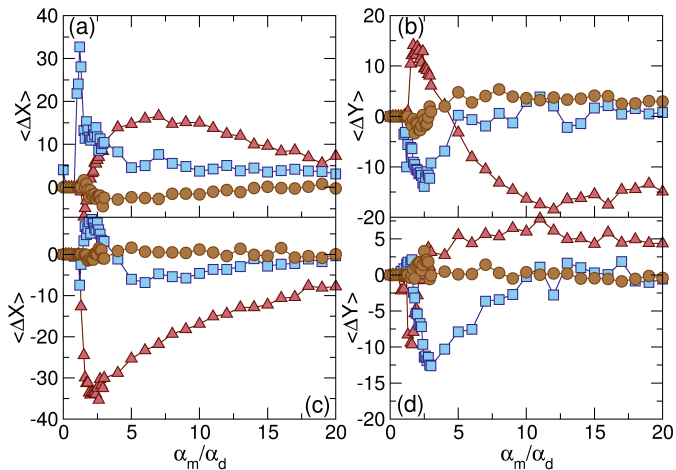
FIG. 14: Ratchet motion in the different arrays illustrated in Fig. 1: conformal pinning array (red triangles), square gradient array (blue squares), and random gradient array (brown circles), in samples with $n_s/n_p = 0.3$. (a) $\langle \Delta X \rangle$ and (b) $\langle \Delta Y \rangle$ after 400 ac cycles vs α_m/α_d for x direction driving F_x^{ac}. (c) $\langle \Delta X \rangle$ and (d) $\langle \Delta Y \rangle$ after 400 ac cycles vs α_m/α_d for y direction driving F_y^{ac}.

The ac drive is strong enough that, during the positive portion of the ac cycle in Fig. 13(c), the skyrmions can pass through the densely pinned regions, and the resulting Hall angle is larger than that observed at the lower ac amplitude of $F_y^{ac} = 0.013$. During the negative portion of the ac cycle, shown in Fig. 13(d), the skyrmions continue to pass through the densely pinned regions, but since the negative x direction is the easy flow direction of the substrate asymmetry, the net amount of negative x motion is increased compared to that which occurs during the positive portion of the ac cycle, and correspondingly the amount of motion in the negative y direction is decreased. Thus, for fixed pinning strength and skyrmion density, the ratchet flow rotates with increasing ac amplitude F_y^{ac} due to the depinning process in the x direction and the increasing Hall angle, as shown in Fig. 1.

VII. SQUARE AND RANDOM GRADIENT ARRAYS

In Fig. 14(a,b) we show $\langle \Delta X \rangle$ and $\langle \Delta Y \rangle$ after 400 ac cycles versus α_m/α_d in samples with $n_s/n_p = 0.3$ containing either the square gradient array illustrated in Fig. 1(b) or the random gradient array shown in Fig. 1(c). Also shown for comparison is a sample with a conformal array. Here the square gradient array produces a large ratchet flux for low $\alpha_m/\alpha_d < 5.0$, and in some cases the flow is in the opposite direction to that observed in the conformal array. The random gradient array in general shows a much smaller ratchet flux that is primarily in the negative x and positive y directions, which is opposite to the flux observed for the conformal array. Fig-

ure 14(c) shows $\langle \Delta X \rangle$ vs α_m/α_d for the same systems under y direction ac driving, F_y^{ac}. In this case, the conformal array always produces a negative x ratchet flux, while the square gradient array shows a weaker ratchet flux as well as a reversal from positive x to negative x flow near $\alpha_m/\alpha_d = 5.0$. The random gradient array does not show any appreciable ratchet flux. In Fig. 14(d), the corresponding $\langle \Delta Y \rangle$ versus α_m/α_d plot indicates that the ratchet flux of the square gradient array is comparable to or even higher than that of the conformal array for $\alpha_m/\alpha_d < 5$, while the random gradient array shows almost no ratchet flux. We observe similar effects for fixed α_m/α_d and varied ac amplitude F^{ac}. In general, the conformal array produces the largest ratchet flux, while the ratchet flux for the square gradient array is weaker, and that of the random gradient array is the weakest.

VIII. SUMMARY

We have shown that ac driven skyrmions interacting with two-dimensional gradient pinning arrays represent a realization of a new type of ratchet system that we call a vector ratchet. In overdamped systems, the ratchet flux is limited to flowing parallel to the substrate asymmetry direction in the forward or reverse direction. In contrast, the strongly non-dissipative Magnus term found in skyrmion systems produces a skyrmion Hall angle that couples the motion parallel and perpendicular to the substrate asymmetry direction. The resulting dc ratchet drift generated by the ac drive can be described as a vector which can rotate counter-clockwise or clockwise in the $x - y$ plane as the ac amplitude or the ratio of the Magnus term to the dissipative term is varied, so that it is possible to realize reversals in the ratchet flux in both the x and y directions. We show that this vector ratchet appears for ac driving both parallel to and perpendicular to the substrate asymmetry direction. The ratchet reversals we observe are a result of collective skyrmion interactions, as previous work on individual skyrmions interacting with asymmetric substrates showed no ratchet reversals. In addition to reversals in the ratchet flux in the x and y directions, the angular rotation of the ratchet vector itself can also show a reversal. We find that it is possible to have rotations of the ratchet vector of up to $360°$, indicating that vector ratchets can be used to direct skyrmion motion in any in-plane direction. Thus, the vector ratchet could serve as a powerful new method for controlling skyrmion motion. Vector ratchets should be general to systems of collectively interacting particles driven over asymmetric substrates where Magnus type effects are present.

1 P. Reimann, Brownian motors: noisy transport far from equilibrium, Phys. Rep. **361**, 57 (2002).

2 P. Hänggi and F. Marchesoni, Artificial Brownian motors: Controlling transport on the nanoscale, Rev. Mod. Phys. **81**, 387 (2009).

3 C.S. Lee, B. Jankó, I. Derényi, and A.L. Barabási, Reducing vortex density in superconductors using the 'ratchet effect,' Nature (London) **400**, 337 (1999).

4 B.L.T. Plourde, Nanostructured superconductors with asymmetric pinning potentials: Vortex ratchets, IEEE Trans. Appl. Supercond. **19**, 3698 (2009).

5 V. A. Shklovskij and O. V. Dobrovolskiy, Frequency-dependent ratchet effect in superconducting films with a tilted washboard pinning potential, Phys. Rev. B **84**, 054515 (2011).

6 J.F. Wambaugh, C. Reichhardt, C.J. Olson, F. Marchesoni, and F. Nori, Superconducting fluxon pump and lenses, Phys. Rev. Lett. **83**, 5106 (1999).

7 C.J. Olson, C. Reichhardt, B Jankó, and F. Nori, Collective interaction-driven ratchet for transporting flux quanta, Phys. Rev. Lett. **87**, 177002 (2001).

8 N.S. Lin, T.W. Heitmann, K. Yu, B.L.T. Plourde, and V.R. Misko, Rectification of vortex motion in a circular ratchet channel, Phys. Rev. B **84**, 144511 (2011).

9 A. Palau, C. Monton, V. Rouco, X. Obradors, and T. Puig, Guided vortex motion in $YBa_2Cu_3O_7$ thin films with collective ratchet pinning potentials, Phys. Rev. B **85**, 012502 (2012).

10 J.E. Villegas, S. Savel'ev, F. Nori, E.M. Gonzalez, J.V. Anguita, R. García, and J.L. Vicent, A superconducting reversible rectifier that controls the motion of magnetic flux quanta, Science **302**, 1188 (2003).

11 C.J. Olson Reichhardt and C. Reichhardt, Rectification and flux reversals for vortices interacting with triangular traps, Physica C **432**, 125 (2005).

12 C.C. de Souza Silva, J. van de Vondel, M. Morelle, and V.V. Moshchalkov, Controlled multiple reversals of a ratchet effect, Nature (London) **440**, 651 (2006).

13 Q. Lu, C.J.O. Reichhardt, and C. Reichhardt, Reversible vortex ratchet effects and ordering in superconductors with simple asymmetric potential arrays, Phys. Rev. B **75**, 054502 (2007).

14 L. Dinis, E.M. González, J.V. Anguita, J.M.R. Parrondo, and J.L. Vicent, Lattice effects and current reversal in superconducting ratchets, New J. Phys. **9**, 366 (2007).

15 D. Perez de Lara, M. Erekhinsky, E.M. Gonzalez, Y.J. Rosen, I.K. Schuller, and J.L. Vicent, Vortex ratchet reversal: Role of interstitial vortices, Phys. Rev. B **83**, 174507 (2011); **87**, 099902 (2013).

16 E.M. Gonzalez, N.O. Nunez, J.V. Anguita, and J.L. Vicent, Transverse rectification in superconducting thin films with arrays of asymmetric defects, Appl. Phys. Lett. **91**, 062505 (2007).

17 L. Dinis, D. Perez de Lara, E.M. Gonzalez, J.V. Anguita, J.M.R. Parrondo, and J.L. Vicent, Transverse ratchet effect and superconducting vortices: simulation and experiment, New J. Phys. **11**, 073046 (2009).

18 C. Reichhardt and C.J.O. Reichhardt, Transverse ac-driven and geometric ratchet effects for vortices in conformal crystal pinning arrays, Phys. Rev. B **93**, 064508 (2016).

19 V. A. Shklovskij, V.V. Sosedkin, and O. V. Dobrovolskiy, Vortex ratchet reversal in an asymmetric washboard pinning potential subject to combined dc and ac stimuli, J. Phys.: Condens. Matter **26**, 025703 (2014).

20 J. Rousselet, L. Salome, A. Ajdari, and J. Prost, Directional motion of brownian particles induced by a periodic asymmetric potential, Nature (London) **370**, 446 (1994).

21 K. Xiao, Y. Roichman, and D.G. Grier, Two-dimensional optical thermal ratchets based on Fibonacci spirals, Phys. Rev. E **84**, 011131 (2011).

22 S. Mühlbauer, B. Binz, F. Jonietz, C. Pfleiderer, A. Rosch, A. Neubauer, R. Georgii, and P. Böni, Skyrmion lattice in a chiral magnet, Science **323**, 915 (2009).

23 X.Z. Yu, Y. Onose, N. Kanazawa, J.H. Park, J.H. Han, Y. Matsui, N. Nagaosa, and Y. Tokura, Real-space observation of a two-dimensional skyrmion crystal, Nature **465**, 901 (2010).

24 N. Nagaosa and Y. Tokura, Topological properties and dynamics of magnetic skyrmions, Nature Nanotech. **8**, 899 (2013).

25 J. Zang, M. Mostovoy, J.H. Han, and N. Nagaosa, Dynamics of skyrmion crystals in metallic thin films, Phys. Rev. Lett. **107**, 136804 (2011).

26 T. Schulz, R. Ritz, A. Bauer, M. Halder, M. Wagner, C. Franz, C. Pfleiderer, K. Everschor, M. Garst, and A. Rosch, Emergent electrodynamics of skyrmions in a chiral magnet, Nature Phys. **8**, 301 (2012).

27 X.Z. Yu, N. Kanazawa, W.Z. Zhang, T. Nagai, T. Hara, K. Kimoto, Y. Matsui, Y. Onose, and Y. Tokura, Skyrmion flow near room temperature in an ultralow current density, Nature Commun. **3**, 988 (2012).

28 J. Iwasaki, M. Mochizuki, and N. Nagaosa, Universal current-velocity relation of skyrmion motion in chiral magnets, Nature Commun. **4**, 1463 (2013).

29 D. Liang, J.P. DeGrave, M.J. Stolt, Y. Tokura, and S. Jin, Current-driven dynamics of skyrmions stabilized in MnSi nanowires revealed by topological Hall effect, Nature Commun. **6**, 8217 (2015).

30 S. Woo, K. Litzius, B. Kruger, M.Y. Im, L. Caretta, K. Richter, M. Mann, A. Krone, R.M. Reeve, M. Weigand, P. Agrawal, I. Lemesh, M.A. Mawass, P. Fischer, M. Klaui, and G.R.S.D. Beach, Observation of room-temperature magnetic skyrmions and their current-driven dynamics in ultrathin metallic ferromagnets, Nature Mater. **15**, 501 (2016).

31 S.-Z. Lin, C. Reichhardt, C. Batista, and A. Saxena, Particle model for skyrmions in metallic chiral magnets: Dynamics, pinning, and creep, Phys. Rev. B **87**, 214419 (2013).

32 J. Müller and A. Rosch, Capturing of a magnetic skyrmion with a hole, Phys. Rev. B **91**, 054410 (2015).

33 C. Reichhardt, D. Ray, and C.J.O. Reichhardt, Quantized transport for a skyrmion moving on a two-dimensional periodic substrate, Phys. Rev. B **91**, 104426 (2015).

34 C. Reichhardt, D. Ray, and C.J.O. Reichhardt, Collective

transport properties of driven skyrmions with random disorder, Phys. Rev. Lett. **114**, 217202 (2015).

[35] W. Jiang, X. Zhang, G. Yu, W. Zhang, X. Wang, M.B. Jungfleisch, J.E. Pearson, X. Cheng, O. Heinonen, K.L. Wang, Y. Zhou, A. Hoffmann, and S.G.E. te Velthuis, Direct observation of the skyrmion Hall effect, Nature Phys. **13**, 162 (2017). doi:10.1038/nphys3883

[36] K. Litzius, I. Lemesh, B. Krüger, P. Bassirian, L. Caretta, K. Richter, F. Büttner, K. Sato, O.A. Tretiakov, J. Förster, R.M. Reeve, M. Weigand, I. Bykova, H. Stoll, G. Schütz, G.S.D. Beach, and M. Kläui, Skyrmion Hall effect revealed by direct time-resolved X-ray microscopy, Nature Phys. **13**, 170 (2017).

[37] W. Jiang, P. Upadhyaya, W. Zhang, G. Yu, M.B. Jungfleisch, F.Y. Fradin, J.E. Pearson, Y. Tserkovnyak, K.L. Wang, O. Heinonen, S.G.E. te Velthuis, and A. Hoffmann, Blowing magnetic skyrmion bubbles, Science **349**, 283 (2015).

[38] Y. Tokunaga, X.Z. Yu, J.S. White, H.M. Rønnow, D. Morikawa, Y. Taguchi, and Y. Tokura, A new class of chiral materials hosting magnetic skyrmions beyond room temperature, Nature Commun. **6**, 7638 (2015).

[39] A. Fert, V. Cros, and J. Sampaio, Skyrmions on the track, Nature Nanotechnol. **8**, 152 (2013).

[40] C. Reichhardt, D. Ray and C.J.O. Reichhardt, Magnus-induced ratchet effects for skyrmions interacting with asymmetric substrates, New J. Phys. **17**, 073034 (2015).

[41] C. Reichhardt, D. Ray, and C.J.O. Reichhardt, Reversible ratchet effects for vortices in conformal pinning arrays Phys. Rev. B **91**, 184502 (2015).

[42] Q. Li, J. Toner, and D. Belitz, Skyrmion versus vortex flux lattices in p-wave superconductors, Phys. Rev. B **79**, 014517 (2009).

[43] J. Garaud and E. Babaev, Skyrmionic state and stable half-quantum vortices in chiral p-wave superconductors, Phys. Rev. B **86**, 060514 (2012).

[44] V.F. Becerra, E. Sardella, F.M. Peeters, and M.V. Milošević, Vortical versus skyrmionic states in mesoscopic p-wave superconductors, Phys. Rev. B **93** 014518 (2016).

[45] B.A. Grzybowski and G.M. Whitesides, Dynamic aggregation of chiral spinners, Science **296**, 718 (2002).

[46] L.J. Hou, Z.L. Misković, A. Piel, and P.K. Shukla, Brownian dynamics of charged particles in a constant magnetic field, Phys. Plasmas **16**, 053705 (2009).

[47] T. Ott, H. Löwen, and M. Bonitz, Magnetic field blocks two-dimensional crystallization in strongly coupled plasmas, Phys. Rev. Lett. **111**, 065001 (2013).

[48] D. Ray, C.J.O. Reichhardt, B. Jankó, and C. Reichhardt, Strongly enhanced pinning of magnetic vortices in type-II superconductors by conformal crystal arrays, Phys. Rev. Lett. **110**, 267001 (2013).

[49] D. Ray, C. Reichhardt, and C.J.O. Reichhardt, Pinning, ordering, and dynamics of vortices in conformal crystal and gradient pinning arrays, Phys. Rev. B **90**, 094502 (2014).

[50] Y.L. Wang, M.L. Latimer, Z.L. Xiao, R. Divan, L.E. Ocola, G.W. Crabtree, and W.K. Kwok, Enhancing the critical current of a superconducting film in a wide range of magnetic fields with a conformal array of nanoscale holes, Phys. Rev. B **87**, 220501(R) (2013).

[51] S. Guenon, Y.J. Rosen, A.C. Basaran, and I.K. Schuller, Highly effective superconducting vortex pinning in conformal crystals, Appl. Phys. Lett. **102**, 252602 (2013).

[52] A.A. Thiele, Steady-state motion of magnetic domains, Phys. Rev. Lett. **30**, 230 (1973).